AIP | Journal of Applied Physics

Nonradiative lifetime extraction using power-dependent relative photoluminescence of III-V semiconductor double-heterostructures

A. W. Walker, S. Heckelmann, C. Karcher, O. Höhn, C. Went, M. Niemeyer, A. W. Bett, and D. Lackner

Articles you may be interested in

Investigation of proton damage in III-V semiconductors by optical spectroscopy
J. Appl. Phys. **119**, 235702 (2016); 10.1063/1.4953585

Temperature dependence of the photoluminescence polarization of ordered III-V semiconductor alloys
J. Appl. Phys. **119**, 115702 (2016); 10.1063/1.4944436

Effect of n-p-n heterostructures on interface recombination and semiconductor laser cooling
J. Appl. Phys. **108**, 113118 (2010); 10.1063/1.3517144

Direct determination of the free-carrier injection density, the free-carrier absorption, and the recombination factors in double heterostructure diodes by optical phase measurements. Part III
J. Appl. Phys. **97**, 123536 (2005); 10.1063/1.1935741

Structural engineering of ferromagnetism in III–V digital ferromagnetic heterostructures
J. Appl. Phys. **95**, 4922 (2004); 10.1063/1.1667594

AIP | Applied Physics Reviews

NEW Special Topic Sections

NOW ONLINE
Lithium Niobate Properties and Applications:
Reviews of Emerging Trends

AIP | Applied Physics Reviews

Nonradiative lifetime extraction using power-dependent relative photoluminescence of III-V semiconductor double-heterostructures

A. W. Walker,[a),b)] S. Heckelmann,[b)] C. Karcher,[c)] O. Höhn, C. Went,[d)] M. Niemeyer, A. W. Bett, and D. Lackner
Fraunhofer Institute for Solar Energy Systems ISE, Heidenhofstraße 2, 79110 Freiburg, Germany

A power-dependent relative photoluminescence measurement method is developed for double-heterostructures composed of III-V semiconductors. Analyzing the data yields insight into the radiative efficiency of the absorbing layer as a function of laser intensity. Four GaAs samples of different thicknesses are characterized, and the measured data are corrected for dependencies of carrier concentration and photon recycling. This correction procedure is described and discussed in detail in order to determine the material's Shockley-Read-Hall lifetime as a function of excitation intensity. The procedure assumes 100% internal radiative efficiency under the highest injection conditions, and we show this leads to less than 0.5% uncertainty. The resulting GaAs material demonstrates a 5.7 ± 0.5 ns nonradiative lifetime across all samples of similar doping (2–3×10^{17} cm^{-3}) for an injected excess carrier concentration below 4×10^{12} cm^{-3}. This increases considerably up to longer than 1 μs under high injection levels due to a trap saturation effect. The method is also shown to give insight into bulk and interface recombination. © 2016 Author(s). All article content, except where otherwise noted, is licensed under a Creative Commons Attribution (CC BY) license (http://creativecommons.org/licenses/by/4.0/). [http://dx.doi.org/10.1063/1.4945772]

I. INTRODUCTION

Characterizing the material quality of III-V semiconductors is essential in understanding and optimizing the performance of optoelectronic devices such as light emitting diodes, photodetectors, semiconductor lasers, and solar cells. The primary metric for material quality is the nonradiative lifetime of minority carriers in the active region, which is dictated by defect-driven Shockley-Read-Hall (SRH) and interface recombination processes. Absolute electroluminescence measurements have shown potential to gauge the material quality by deducing the internal radiative efficiency.[1] In this technique, the internal radiative efficiency can be extracted using a generalized optoelectronic model of multijunction solar cells.[2] However, careful calibration of the optical setup is required to achieve high accuracy in determining the absolute photon emission, i.e., the external radiative efficiency. Furthermore, knowledge of the optical properties of the multi-layer device is required to relate the measured external radiative efficiency to an internal radiative efficiency. On the other hand, photoluminescence (PL)-based measurements offer simple yet effective methods of probing these carrier recombination dynamics in III-V semiconductors. So far, time-resolved photoluminescence (TRPL) has proved to be effective in gauging these processes quantitatively.[3,4] This method requires ultra-fast lasers and picosecond resolved photodetectors, which are both

sensitive and expensive, and therefore, requires thorough calibration procedures. In this paper, it is shown that a simple, fast and contactless **p**ower-**d**ependent **r**elative **p**hoto**l**uminescence (PDR-PL) measurement of a double-heterostructure (DH) is sufficient to quantify the bulk minority carrier nonradiative recombination lifetime and surface recombination velocity. The methodology and theory of PDR-PL are described to enable the extraction of these nonradiative recombination parameters. This leads to a fast and powerful technique for monitoring the condition of a crystal growth reactor and process optimization that can be applied in most existing PL setups.

The internal radiative efficiency, which relates the radiative recombination rate to the total recombination rate, is a measure of the intrinsic material quality.[5–7] However, the influence of photon recycling in PL-based measurements must be considered when deriving the internal radiative efficiency, since it has been shown previously that the thickness of the emitting material influences the photon recycling factor and thus the observed radiative lifetime.[8] Furthermore, the optical properties of the rear-side of the analysed device, such as the presence of a rear-side mirror directly below the emitting material, strongly influence the effective radiative recombination coefficient by enhancing the reabsorption of the internal photoluminescence.[9] Thus, the effective radiative recombination coefficient, which is described in Ref. 9, is a device-dependent parameter and differs from the Einstein coefficient for spontaneous emission, which is solely a material-dependent parameter. Therefore, the effects of reabsorption must explicitly be accounted for in quantifying the internal radiative efficiency of a DH from PL-based measurements. In order to do so, the optical properties of the system must be carefully evaluated to estimate the photon

escape probabilities to the front-side as well as to the rear-side. The external radiative efficiency depends solely on the photons escaping the front-side of the structure. It is typically probed using absolute electroluminescence to gauge the internal radiative efficiency of the material. However, when probing the DH with the newly introduced power dependent relative PL measurement, this paper demonstrates that the escape probabilities into the substrate must also be accounted for. This is primarily because the thickness strongly influences the reabsorption after total internal reflection from the semiconductor/air interface prior to the inevitable transmission into the substrate. These effects are considered by modeling an effective radiative recombination coefficient which accounts for re-absorption and escape through both front- and rear-sides of the DH. Thus, the overall method gauges not the external radiative efficiency but an effective radiative efficiency, which is defined as the probability an electron-hole pair is emitted and subsequently escapes either through the front- or rear-side of the structure.

Section II outlines the structural details of the analyzed samples, along with the experimental procedure and qualitative results on a *p*-type AlGaAs/GaAs/AlGaAs DH. In Section III, the theory explaining the measurement results is derived. First, the steady-state theory is discussed, whereby the measured (integrated) PL-signal intensity is shown to be a linear function of the excitation power in both low and high carrier injection regimes at room temperature. The ratio of low to high injection PL-signals is then shown to give direct access to the nonradiative lifetime in the low injection regime. However, the radiative recombination coefficient which is needed in the procedure to compute the radiative recombination rate must account for the influence of photon recycling, which depends on both thickness[8] and on the optical properties of the system.[9] The detailed discussion on such an effective radiative coefficient used to compute the effective radiative efficiency is given in Section III B. To validate the model, four GaAs DH samples of various thicknesses are characterized, and the nonradiative lifetimes are extracted. This analysis is carried out in Section IV. Conclusions are then given in Section V. Appendices A and B then provide insight into the relevant recombination processes over injection, and the separation of bulk and interface effects respectively.

II. STRUCTURAL DETAILS AND EXPERIMENTAL PROCEDURE

Fig. 1 illustrates the structural details of the investigated DHs, composed of an AlGaAs/GaAs/AlGaAs layer stack grown on GaAs substrates with a 6° offcut towards the [111] B direction. Nine periods of strain-balanced quantum well structures composed of $Ga_{0.60}In_{0.40}P/Ga_{0.85}In_{0.15}As/Ga_{0.60}In_{0.40}P$ are grown between the DH and the GaAs semi-insulating substrate to minimize luminescence coupling between the GaAs test layer and the substrate. Four DH structures with different test layer thicknesses were grown and characterized to distinguish between the influence of bulk and surface recombination velocity in the system. No anti-reflection coating was deposited on the structures.

10 nm	*i*-GaAs	cap	-
100 nm	*p*-Al$_{0.75}$Ga$_{0.25}$As:Zn	barrier	4.0E17 cm^{-3}
d	*p*-GaAs:Zn	test layer	3.0E17 cm^{-3}
100 nm	*p*-Al$_{0.75}$Ga$_{0.25}$As:Zn	barrier	4.0E17 cm^{-3}
25 nm	*i*-Ga$_{0.60}$In$_{0.40}$P	QW-barrier	-
33 nm	*i*-Ga$_{0.85}$In$_{0.15}$As	QW	-
25 nm	*i*-Ga$_{0.60}$In$_{0.40}$P	QW-barrier	-
450 µm	SI-GaAs	substrate	-

×9

FIG. 1. Structural details of an AlGaAs/GaAs/AlGaAs double heterostructures grown on a GaAs semi-insulating substrate with strain-balanced Ga$_{0.60}$In$_{0.40}$P/Ga$_{0.85}$In$_{0.15}$As/Ga$_{0.60}$In$_{0.40}$P quantum wells (QWs). The thickness of the test layer (*d*) has been varied.

The GaAs DHs are illuminated with a 532 nm laser light with incident intensity ranging from 1 to 10^8 W/m^2 to probe the photoluminescence intensity over a wide range of injection levels. As the laser intensity increases, the material's internal radiative efficiency is expected to increase, which is reflected in the recombination lifetime of the carriers, where this is defined by

$$\frac{1}{\tau} = \frac{1}{\tau_{rad}} + \frac{1}{\tau_{srh}} + \frac{1}{\tau_{Auger}}, \quad (1)$$

where τ_{rad} is the radiative lifetime, τ_{srh} is the nonradiative Shockley-Read-Hall (SRH) lifetime (which accounts for both bulk and interface recombination), and τ_{Auger} is the lifetime according to Auger recombination. Assuming the Auger recombination is negligible, the nonradiative SRH lifetime may vary as a function of injection due to effects such as trap saturation.[10] Considering the radiative lifetime (τ_{rad}), it can be approximated as

$$\tau_{rad} \cong \frac{1}{B_{rad}(N_{A,D} + \Delta n)}, \quad (2)$$

where B_{rad} is the radiative recombination coefficient, $N_{A,D}$ is the doping concentration for a *p*- or *n*-doped sample, respectively, and Δn is the excess carrier concentration (which corresponds to the injection level). The radiative lifetime, therefore, remains constant under low injection when $N_{A,D} \gg \Delta n$ but decreases when the injection approaches the doping concentration. Exploring a wide range of injection levels thus probes low to high injection regimes where the effective lifetime will vary. The relative integrated PL (i.e., the integrated PL-signal divided by the incident laser light intensity) is illustrated as a function of laser light intensity in Fig. 2, where it is normalized to the maximum measured relative integrated PL-signal to obtain a power-dependent relative PL (or PDR-PL) profile. Three regimes are visible in the measured data of Fig. 2: (I) the low injection regime outlined as a plateau between 1 and 2×10^2 W/m^2, (II) an intermediate regime between 2×10^2 and 4×10^6 W/m^2 whereby radiative recombination becomes more and more dominant in the material, and (III) the high injection regime where the material can be approximated to be in a purely radiative
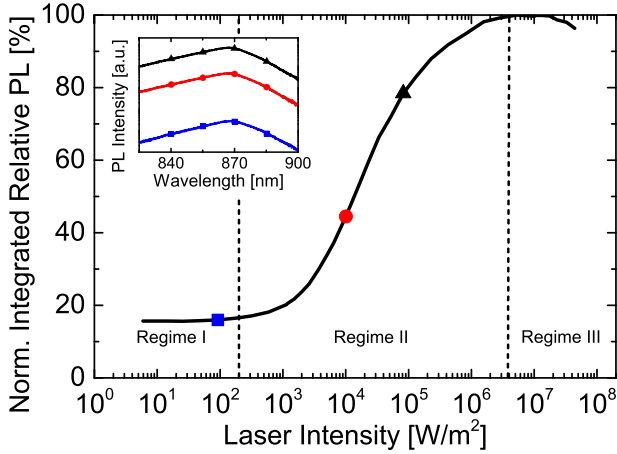
FIG. 2. Measured integrated relative PL (i.e., divided by laser power) normalized to the maximum measured integrated PL for a 1000 nm GaAs DH as a function of 532 nm laser intensity. Inset plot shows the logarithm of the PL intensity for three laser intensities. The integrated PL measurements correspond to the three data points on the main plot according to their respective symbols.

state. If no losses were encountered under high injection, the signal would remain flat for increasing laser intensities in regime III. However, a drop in signal is observed under the highest illumination intensities. This is determined to be mostly due to the Auger recombination (see Appendix A). Conduction band filling effects may contribute about 0.2% to the observed drop, since electrons in the conduction band get scattered into the L-band valley, where they experience a significantly lower radiative recombination probability. Carrier loss due to electrons escaping the DH over the barrier height is far less probable (see Appendix A).

The shape of the PDR-PL profile is flat in regime I primarily because traps which mediate Shockley-Read-Hall recombination are abundant compared to the excess carrier concentration. As the injection level increases, these traps begin to saturate,[10] thus increasing the fraction of excess carriers recombining radiatively. Fig. 2 shows a single S-shape, which is indicative of a single trap population being saturated. However, other samples may demonstrate a double S-shape, which may indicate that two trap populations are saturated at different injection levels.

III. THEORETICAL BACKGROUND

A. Steady-state conditions

The illumination of a DH by a cw laser with intensity I_{laser} probes the system under steady state, whereby the continuity equation for electrons is given by

$$\frac{\partial n}{\partial t} = q \nabla \cdot \bar{J} + G - U = 0, \qquad (3)$$

where G and U are the generation and recombination rates, respectively, $\bar{J}$ is the current, q is the electronic charge, and n is the electron concentration. Since the DH is at open circuit (i.e., no net current is flowing) because no electrical contacts are established, the steady-state equation

reduces to balancing generation rates with recombination rates as

$$G = \frac{I_{laser} A_{DH}}{E_{ph} d} = U_{rad} + U_{srh} + U_{Auger}, \qquad (4)$$

where the generation rate is expressed based on the absorption of the laser where d is the thickness of the absorbing test layer of the DH, E_{ph} represents the photon energy of the excitation laser, and A_{DH} is the relative absorption in the test layer of the DH. The relative absorption accounts for the reflection and transmission of the laser light incident on the sample surface, and can be computed using the transfer matrix formalism.[11] Note that the absorption in the barrier layers can contribute to carrier concentration in the absorber layer, but this is not accounted for in the model. Finally, U_{rad}, U_{srh}, and U_{Auger} represent the radiative, the nonradiative SRH (both bulk and interface), and the Auger recombination rates, respectively.

The nonradiative SRH recombination rate can be computed using standard SRH theory as[12]

$$U_{srh} = \frac{np - n_i^2}{\tau_n(p + p_t) + \tau_p(n + n_t)} \cong \frac{\Delta n}{\tau_n + \frac{\Delta n}{N_A}\tau_p}, \qquad (5)$$

where $n = n_o + \Delta n$ and $p = N_A + \Delta n$ are the electron and hole concentrations, respectively, n_o and n_i are the equilibrium electron concentration and the intrinsic carrier concentration, respectively, τ_n (τ_p) is the electron (hole) nonradiative lifetime, and n_t and p_t are the electron and hole trap concentrations, both of which can be neglected assuming $p_t, n_t \ll p$. In the example of a p-doped sample in low injection, one can assume that $N_A \gg \Delta n$, and so the lifetime is determined by the minority carrier lifetime (τ_n). This allows for the adoption of an nonradiative SRH lifetime $\tau_{srh} = \tau_{srh}(\Delta n) = \tau_n + \frac{\Delta n}{N_A}\tau_p$. Note that with this simplification, trap saturation effects are not explicitly accounted for, and will instead appear as an injection level dependent $\tau_{srh}(\Delta n)$. Surface recombination is implicit in Equation (5) via this nonradiative lifetime. The separation of bulk and interface recombination is discussed in Appendix B.

The recombination rate due to Auger processes is accounted for using[13]

$$U_{Auger} = C_{Auger}(n + p)(np - n_i^2), \qquad (6)$$

where C_{Auger} is the Auger recombination coefficient (material specific: 10^{-30} cm^6 s^{-1} for GaAs[14]) and is assumed to be the same for both carrier types. Using this value, the Auger recombination does not have an important role in dictating the overall recombination rates until the highest injection levels ($\sim 10^8$ W/m^2) are reached for GaAs, at which point it may contribute up to 1–3% of the total recombination rates (see Appendix A).

Finally, the radiative recombination rate is given by

$$U_{rad} = B_{rad}(np - n_i^2). \qquad (7)$$

Note that simplifying Equation (7) for a uniformly doped material reduces to Equation (2) if one assumes a form $U_{rad} = \Delta n / \tau_{rad}$. It is important to note that care must be taken in interpreting the parameter B_{rad} for any structure, because it cannot be considered as a material constant in PL-based measurements since it is strongly influenced by photon recycling.[9,15] For example, the thickness of the DH, its cladding layers, the presence of an anti-reflection coating, and the substrate/back mirror configuration will play a strong role in the strength of the photon recycling effect. This results in an effective radiative recombination coefficient B_{rad}^{eff} that is observed in the PL-based measurements and is adopted in this study. The calculation of this structure-dependent parameter is discussed in more detail in Section III B in order to compute an effective radiative recombination rate U_{rad}^{eff} analogous to Equation (7).

The measured PL-intensity, I_{PL}, is based on the fraction of photons emitted by the DH, which is not entirely collected due to losses into the substrate and due to various optical losses in the measurement set-up. Thus, it can be expressed using a fraction of the true total integrated PL, and it can be described by the number of generated electron-hole pairs that recombine radiatively at a photon energy $E_{ph}^{PL}(\lambda)$ throughout the emitting region scaled by a wavelength-dependent optical factor $C(\lambda)$ that accounts for these two aforementioned losses. In general, this is expressed as

$$I_{PL}(I_{laser}) = d \int C(\lambda) E_{ph}^{PL}(\lambda) b(\lambda) U_{rad}^{eff} d\lambda, \qquad (8)$$

where $b(\lambda)$ is a normalized PL-lineshape distribution function (see the inset of Fig. 2). The optical loss factor in Equation (8) is independent of laser intensity, since the relative probability of photons escaping the front to the rear-side remains constant. Equation (8) can be re-written using the generation rate from Equation (4) as

$$I_{PL}(I_{laser}) = d \int C(\lambda) E_{ph}^{PL}(\lambda) b(\lambda) U_{rad}^{eff} \frac{G}{U_{rad}^{eff} + U_{srh} + U_{Auger}} d\lambda, \qquad (9a)$$

$$I_{PL}(I_{laser}) = d \frac{I_{laser} A_{DH}}{E_{ph}^{laser}} \eta_{eff}(I_{laser}) \int C(\lambda) E_{ph}^{PL}(\lambda) b(\lambda) d\lambda, \qquad (9b)$$

where the effective radiative efficiency η_{eff} (assumed to be wavelength independent but dependent on laser intensity) is introduced as

$$\eta_{eff}(I_{laser}) = \frac{U_{rad}^{eff}}{U_{rad}^{eff} + U_{srh} + U_{Auger}}. \qquad (10)$$

Note that Equation (10) typically refers to the internal radiative efficiency. However, U_{rad}^{eff} is an effective radiative recombination rate evaluated using an effective radiative recombination coefficient analogous to Equation (7) which is not the Einstein coefficient for spontaneous emission. Thus, Equation (10) is not the internal radiative efficiency of the material, but the effective radiative efficiency of the device. Equation (9b) illustrates that the measured PL intensity

scales linearly with the laser intensity, assuming the majority of the radiative emission originates from direct transitions of free carriers from the conduction band minimum to the valence band maximum (i.e., minimal radiative transitions via defect states). A nonlinear dependence of the PL intensity as a function of laser intensity is typically observed for transitions via defects, or for samples with gradients in doping concentrations.[16] The former can be neglected for GaAs at room temperature, and the latter is not the case in this study.

The comparison of the measured relative PL signal, $I_{PL}(I_{laser})/I_{laser}$, where the internal radiative efficiency $\eta_{int} < 1$, to the corresponding measured relative PL signal under high injection, assuming $\eta_{int}|_{HI} = 1$, therefore, gives insight into the effective radiative efficiency η_{eff}, as defined in Equation (10), if one ignores any change in the PL photon energy and distribution due to conduction band filling (the Burstein-Moss effect), or

$$\frac{\dfrac{I_{PL}(I_{laser})}{I_{laser}}}{\dfrac{I_{PL}(I_{laser})}{I_{laser}}\bigg|_{HI}} = \eta_{eff}(I_{laser}). \qquad (11)$$

Note that as the internal radiative efficiency approaches unity, the effective radiative efficiency will also approach unity, since all photons will escape the DH. Conversely, the external radiative efficiency will only approach an absolute value of 2–3% due to the relatively small escape cone between semiconductor and air. For a structure with an ideal rear-side reflector directly below the DH, the external radiative efficiency will be equivalent to the effective radiative efficiency. The measurement of the relative integrated PL-signal from low to high injection, therefore, gives a direct insight into the effective radiative efficiency if and only if the highest PL signal measured represents the system approaching an internal radiative efficiency of 1 ($\eta_{int} \to 1$). A simple calculation shows that for a laser intensity of 10^7 W/m^2 operating at 532 nm, as used in the measurements, an injection level of close to 200 A/cm^2 is created assuming a relative absorption of 0.5, which has been calculated to be within the radiative regime.[17] Note that solving the set of coupled equations to determine the overall recombination rates leads to the explicit determination of the effective radiative, SRH and Auger recombination rates with respect to the total recombination rates, thus directly probing the high injection η_{eff}. Since, in general, $\eta_{int} \geq \eta_{eff}$, this initial calculation can subsequently be used in a second iteration of calculations where this high injection η_{eff} re-normalizes the overall PDR-PL signal. We estimate the error in this assumption to be less than 0.5% (see Appendix A).

To compute the excess carrier concentration as a function of laser light intensity, the set of Equations (5)–(7) must be solved numerically in combination with Equations (9b) and (10). The effective radiative efficiency enters the set of equations via Equation (11) and is based directly on the measured data (see Fig. 2). The set of equations can only be solved by expressing the nonradiative SRH lifetime using Equations (5) and (10) as

$$\tau_{\mathrm{srh}} = \frac{\Delta n}{\dfrac{U_{\mathrm{rad}}^{\mathrm{eff}}}{\eta_{\mathrm{eff}}} - U_{\mathrm{rad}}^{\mathrm{eff}} - U_{\mathrm{Auger}}}. \tag{12}$$

Note that Equation (12) gives the nonradiative lifetime which represents the minority carrier lifetime and the influence from the majority carrier lifetime as the excess carrier concentration reaches the same magnitude as the doping (see Equation (5)). The measured PDR-PL signal (Fig. 2), therefore, allows for a direct measure of the nonradiative lifetime as $\eta_{\mathrm{eff}} \to 1$ under high injection.

If one is only interested in the magnitude of the nonradiative lifetime in the low injection regime where minority carrier devices operate (i.e., $\Delta n \ll N_A$), then the recombination rates (namely, Equations (5) and (7) assuming the Auger recombination can be neglected) can be simplified in the following form:

$$U = \frac{\Delta n}{\tau}. \tag{13}$$

Equation (12) can then be re-written directly from the measurement of η_{eff} to calculate the nonradiative lifetime using

$$\tau_{\mathrm{srh}} = \frac{\eta_{\mathrm{eff}} \tau_{\mathrm{rad}}^{\mathrm{eff}}}{1 - \eta_{\mathrm{eff}}}, \tag{14}$$

where $\tau_{\mathrm{rad}}^{\mathrm{eff}}$ is the effective radiative recombination lifetime and is given by Equation (2) using the effective radiative recombination coefficient. This simplification demonstrates that the magnitude of the normalized PDR-PL under low injection (regime I) corresponds directly to the ratio of the nonradiative lifetime to the sum of radiative and nonradiative lifetimes. Note that when the excess carrier concentration approaches the magnitude of the doping concentration, these equations lose accuracy since Δn becomes relevant in Equation (2). Re-arranging Equation (4) using Equations (13) and (14) for both the radiative and nonradiative recombination rates gives an estimate of the carrier concentration as

$$\Delta n = G \frac{\tau_{\mathrm{srh}} \tau_{\mathrm{rad}}^{\mathrm{eff}}}{\tau_{\mathrm{srh}} + \tau_{\mathrm{rad}}^{\mathrm{eff}}}. \tag{15}$$

The theory can then be used to explain the measurements of Fig. 2. In regime I, relatively strong nonradiative recombination is occurring, since traps which mediate the SRH recombination process are quickly capturing both carrier types before any saturation is possible. Furthermore, the effective radiative lifetime $\tau_{\mathrm{rad}}^{\mathrm{eff}}$ is fixed and dictated by the doping concentration, since $\Delta n \ll N_A$ (this can be observed in Fig. 5(b) of Section IV). The radiative lifetime is considerably longer in this regime than under high injection conditions. Regime I is therefore a plateau since it represents a constant effective radiative efficiency marked by constant radiative and nonradiative lifetimes. As the illumination intensity increases beyond $10^3 \, \mathrm{W/m^2}$, a saturation of SRH traps is observed,[10] since the radiative lifetime is still constant ($\Delta n \ll N_A$ is still valid in this range, see Fig. 5(b)).

An intensity of greater than $10^5 \, \mathrm{W/m^2}$ is required to observe a decrease in the radiative lifetime. Such laser intensities probe a regime increasingly dominated by the radiative recombination.

B. Effective radiative recombination coefficient

The effective radiative recombination coefficient, as given in Equation (7), dictates the overall magnitude of the radiative recombination escaping the active layer of the DH. It accounts for reabsorption within the DH as well as the optical influence of the top and bottom interfaces and can be used to compute the effective radiative efficiency. This effective radiative recombination coefficient can be computed using[18]

$$B_{\mathrm{rad}}^{\mathrm{eff}} = \frac{J_{rad,0}}{q d n_i^2}, \tag{16}$$

where $J_{rad,0}$ is the radiative flux emitted by the active layer through the top surface of the structure as well as into the substrate (see Fig. 3(a)). This flux depends on the optical parameters of the structure[9] as well as on the test layer thickness.[8] In order to account for these effects, a grey body is adopted[19] first to calculate the flux $J_{rad,0}^*$ through the top surface of an ideal structure (see Fig. 3(b)), given by

$$J_{rad,0}^* = 2qc \int_{\Omega} \int_0^{\infty} \frac{1}{\lambda^4} \frac{a(\lambda, d)}{e^{\frac{hc}{\lambda k_B T}} - 1} d\lambda \cos \theta d\Omega, \tag{17}$$

where $a(\lambda, d) = \left(1 - R(\lambda)\right)\left(1 - e^{\frac{-2\alpha(\lambda)d}{\cos(\theta)}}\right)$ is the absorptivity of the ideal DH, which assumes a double path length for the absorptivity within the escape cone due to the ideal mirror,
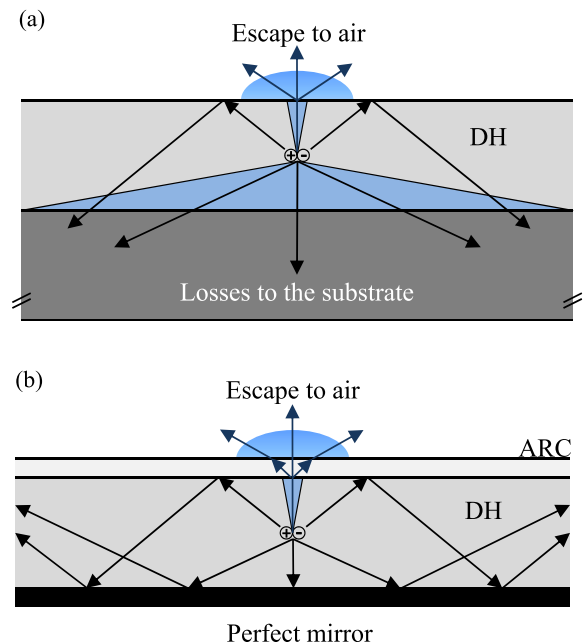
(a)

(b)

FIG. 3. Emission cones from an oscillating point dipole within (a) a DH on substrate and (b) the corresponding ideal DH structure with a perfect back mirror (and hence no escape cone) and an ideal ARC.

and that the Beer-Lambert law is independent of emission angle strictly within the escape cone, i.e., $\cos(\theta < \theta_c) \approx 1$, Ω is the solid angle of emission, and the remaining parameters retain their usual meanings.

To model the total photon escape out of the DH on substrate (both through the front into air and through the rear-side into the substrate), one must relate $J^*_{rad,0}$ for the ideal structure to the real DH on substrate. This can be performed by comparing the total front-side escape in the ideal structure to the total escape out of the real structure. Fig. 3(a) illustrates this idea schematically for a point of emission within an absorbing medium based on escape cones for a DH on substrate. Significant total internal reflection occurs at the top interface (between semiconductor and air) due to the small escape cone of $\sim 16°$ to the normal. Thus, a significant fraction of the photoluminescence is reflected towards the substrate, which has little to no refractive index mismatch compared to the DH. If the substrate is replaced with a perfectly reflective back mirror (Fig. 3(b)), escape through the rear-side can be completely mitigated.[20] The evaluation of Equation (17) for a structure with an ideal back mirror thus yields the total photon flux escaping the ideal DH, since light must escape through the front-side. This is the basis which can be used to evaluate the total escape in the real GaAs DHs of interest. To achieve this, Equation (17) must first be re-written as[21]

$$J_{rad,0} = 2qc \int_\Omega \int_0^\infty \frac{P(\lambda)}{\lambda^4} \frac{a(\lambda,d)}{e^{\frac{hc}{\lambda k_B T}} - 1} d\lambda \cos\theta d\Omega, \qquad (18)$$

where $P(\lambda)$ represents the ratio of the photon fluxes exiting the real DH represented in Fig. 3(a) (both front-side into air and rear-side into the substrate) to the photon fluxes exiting the ideal structure. Note that the evaluation of $P(\lambda)$ accounts for the internal angular emission.[21] The ideal structure, as shown in Fig. 3(b), is an identical structure to the real DH, except that all absorbing layers below the DH (including the substrate, any buffer layers and the MQWs) are replaced with an ideal 100% reflective back mirror. Furthermore, the ideal structure must have an ideal ARC on the top surface to minimize incident reflectivity. The solution to Equation (17) for this ideal structure thus represents the total radiative recombination flux occurring in the ideal DH and emitted through the top surface. Equation (18) simply scales the total radiative recombination flux of the ideal structure by the ratio of the photon fluxes escaping the real DH (including transmission into the substrate and absorption by the MQWs) to the fluxes escaping the ideal structure.

The calculation of $P(\lambda)$ requires a more rigorous optical model such as the scattering matrix method, which can solve for the photon fluxes emitted out of a one-dimensional photonic structure due to an emitting oscillating point dipole within an absorbing layer of the structure.[22,23] Both the real GaAs DH structure and its ideal counter-part must be simulated optically to compute $P(\lambda)$, and with a sufficiently high wavelength resolution; in these examples, a 3 nm resolution is adopted. The absorption in the MQWs is modeled using bulk GaAs absorption data shifted to the band edge of $Ga_{0.85}In_{0.15}As$ (~ 1.29 eV), since the primary purpose of the

MQWs is to absorb the PL of GaAs. The same method is applied to $Ga_{0.60}In_{0.40}P$ using $Ga_{0.50}In_{0.50}P$ absorption data. The scattering-matrix based optical model has previously been adopted to simulate the effects of photon recycling and luminescent coupling in solar cells.[20,24] It is also comparable to that published by Wilkins *et al.*[25] to model luminescent coupling in planar opto-electronic devices.

Fig. 4(a) illustrates the calculated relative front-side and rear-side escaping photon fluxes (integrated over all solid angles) as a function of depth within a 1000 nm GaAs DH with the MQWs and the substrate for three wavelengths relevant to the spontaneous emission of GaAs (see inset of Fig. 2(b)). Wavelengths which are more strongly reabsorbed are less likely to escape through the rear-side, whereas longer wavelengths are significantly more likely to escape. The front-side escape probabilities are maintained below 4% due to the small escape cone from semiconductor to air. The front-side escape exhibits a weak dependence on depth, which becomes stronger for shorter wavelengths due to stronger re-absorption. Fig. 4(b) illustrates both front and rear-side escaping photon fluxes for the same wavelengths in the ideal structure. Note that the fluxes escaping the rear-side are totally diminished due to the ideal reflectivity of the back
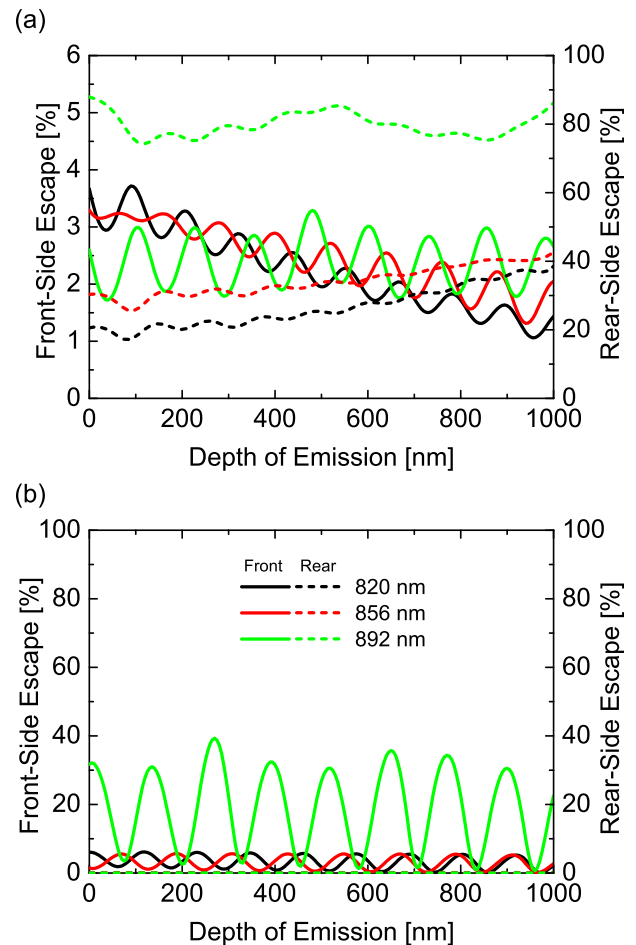
(a)

(b)

FIG. 4. (a) Escape probability as a function of depth of emission within a 1000 nm GaAs DH with a substrate for three wavelengths relevant to the spontaneous emission of GaAs (see inset of (b)), and (b) for an identical GaAs DH but with an ideal mirror rather than a substrate (note there is no escape from the rear-side). Note the different front-side axes for both (a) and (b).

TABLE I. Effective radiative recombination coefficient $B_{\text{rad}}^{\text{eff}}$ and low-level injection lifetime $\tau_{\text{rad}}^{\text{eff}}$ for all four GaAs-DHs using Equation (2).

Sample	DH Thickness (nm)	Doping (cm^{-3})	$J_{rad,0}$ (A cm^{-2})	$B_{\text{rad}}^{\text{eff}}$ (cm^3 s^{-1})	$\tau_{\text{rad}}^{\text{eff}}$ (ns)
DH-1	200	3×10^{17}	3.55×10^{-21}	2.36×10^{-10}	14
DH-2	500	3×10^{17}	5.52×10^{-21}	1.53×10^{-10}	22
DH-3	1000	3×10^{17}	7.77×10^{-21}	1.13×10^{-10}	32
DH-4	2000	2×10^{17}	1.02×10^{-20}	7.50×10^{-11}	61

mirror. The consequence is that all escape is through the front surface, resulting in significantly more overall re-absorption. The oscillations visible in both figures are due to Fabry-Perot interference.

The weighting factor is then computed by integrating the sum of both front-side and rear-side escaping fluxes ($S_{\text{front}}^{\text{DH}}(\lambda, x)$ and $S_{\text{rear}}^{\text{DH}}(\lambda, x)$, respectively) over depth for the real DH, and dividing it by the same integral for the ideal DH $S_{\text{front}}^{\text{ideal}}(\lambda, x)$, or

$$P(\lambda) = \frac{\int \left(S_{\text{front}}^{\text{DH}}(\lambda, x) + S_{\text{rear}}^{\text{DH}}(\lambda, x) \right) dx}{\int \left(S_{\text{front}}^{\text{ideal}}(\lambda, x) \right) dx}. \quad (19)$$

Equation (18) can therefore be solved for each DH structure using Equation (19). Finally, the effective radiative recombination coefficient, which dictates the overall magnitude of the radiative recombination, can be computed using Equation (16). This demonstrates that the effective radiative recombination coefficient (which is related to the lifetime according to Equation (2)) is intricately linked to the DH's overall thickness, and also to the optical properties of the system as dictated by $J_{rad,0}$. Table I summarizes the calculated $J_{rad,0}$, $B_{\text{rad}}^{\text{eff}}$, and effective radiative lifetimes as a function of DH thickness. As the DH increases in thickness, the radiative recombination current density $J_{rad,0}$ increases according to the absorptivity. The $B_{\text{rad}}^{\text{eff}}$, on the other hand, decreases as a function of thickness, thus increasing the effective radiative lifetime from 14 ns to 61 ns (note the doping concentration of each sample). This is a consequence of photon recycling. The values of $B_{\text{rad}}^{\text{eff}}$ are in good agreement with previously reported values,[9,14,26] including the photon recycling factors reported by Lumb. *et al.* for a solar cell without a back side reflector.[27] Note that evaluating Equations (17) and (18) requires accurate absorption coefficients near the band edge, which depend on doping concentration.[14] Furthermore, below-bandgap absorption due to defects should not contribute to emission at room temperature.

IV. RESULTS AND DISCUSSION

To evaluate the robustness and accuracy of the nonradiative lifetime extraction procedure described in Section III, four GaAs DH samples of different thicknesses are grown and characterized by PDR-PL. The measurements for all four samples were performed at room temperature, and measurement conditions were kept constant. Fig. 5(a) illustrates the effective radiative efficiency, which was calculated as
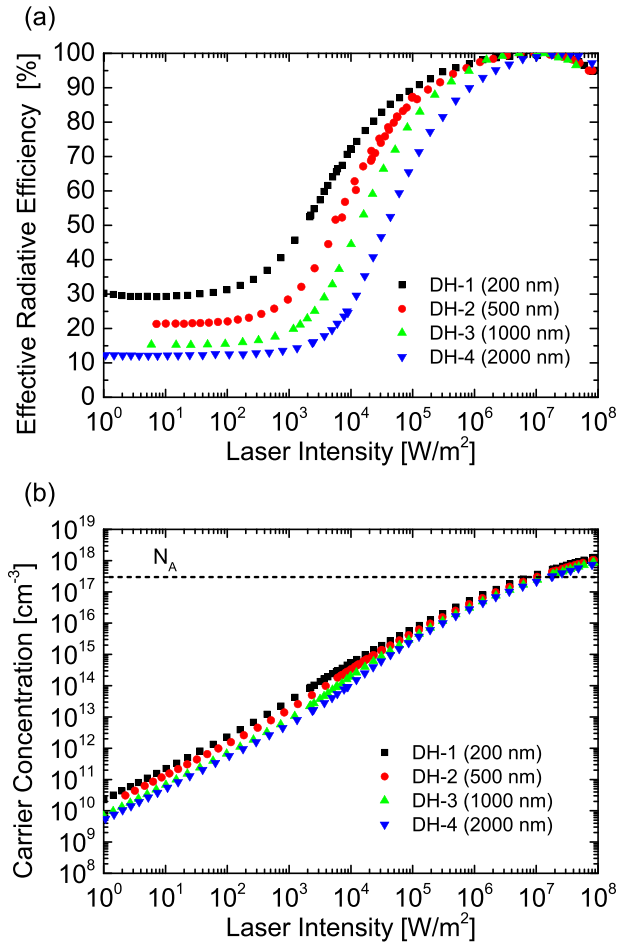

FIG. 5. (a) Measured effective radiative efficiency (η_{eff}) using intensity-dependent photoluminescence, and (b) calculated electron concentrations in four GaAs DHs (200 nm, 500 nm, 1000 nm, and 2000 nm) as a function of the 532 nm laser intensity.

described in Section II. Note that no superlinear behavior has been observed. Under low injection conditions, the sample thickness and radiative efficiencies are inversely proportional. This may seem counter-intuitive at first, since one would expect that the thinnest sample would suffer the most from interface recombination (assuming identical bulk material quality), and would thus have the lowest effective radiative efficiency. However, the main reason for the opposite trend is that the thinnest sample has the shortest effective radiative lifetime (see Table I), and therefore truly has the highest effective radiative efficiency, at least when interface recombination is not significant.

As the injection level increases, the thinner samples increase in effective radiative efficiency the fastest, primarily because of higher carrier concentrations than in the thicker samples. Carrier concentration was calculated by solving the set of Equations (2)–(5) and (10), and can be seen in Fig. 5(b). The higher concentration in the thinner samples at the same excitation level results in a faster saturation of the SRH traps. All samples reach a near-radiative state under high injection, although the thinner samples reach this state at slightly lower intensities. The carrier concentrations, shown in Fig. 5(b), show some convergence under laser intensities greater than 10^5 W/m^2, which
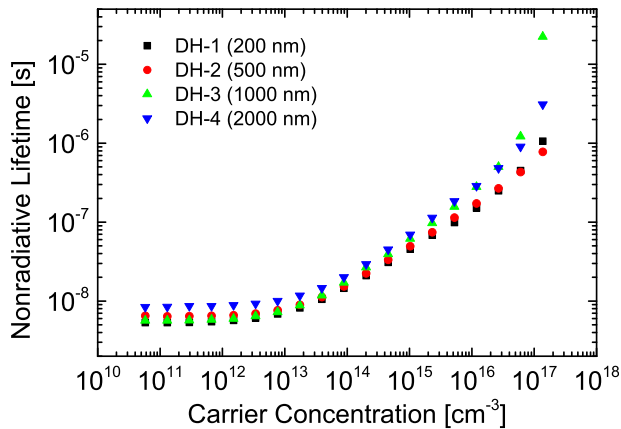
FIG. 6. Extracted nonradiative lifetime using Equation (12) for four GaAs DHs (200 nm, 500 nm, 1000 nm, and 2000 nm) calculated carrier concentration.

is a sign of trap saturation. However, the drop-off in effective radiative efficiency under the highest laser intensities occurs prominently for the thinner structures, since the higher carrier concentrations in these structures result in a stronger Auger recombination.

Upon extracting the nonradiative lifetime using Equation (10), a consistent trend is found whereby the nonradiative lifetime in DH-1–DH-3 converges to 5.7 ± 0.5 ns in the low-injection regime (uncertainty attributed to scatter between samples DH-1–DH-3), as shown in Fig. 6. Note that the nonradiative lifetime is plotted as a function of carrier concentration rather than the laser intensity. This is done to compare the nonradiative lifetimes of all samples directly. The results illustrate that the nonradiative lifetime for sample DH-4 is the longest, primarily because the doping concentration is lower than the other three samples as measured using electrochemical capacitance voltage profiling (2×10^{17} cm^{-3} vs. 3×10^{17} cm^{-3}, see Table I). This demonstrates that lower doping can increase the nonradiative lifetime in *p*-type GaAs (see Figure 3 of Ref. 27, for example). The respective increases in nonradiative lifetime for the thinnest two samples are the weakest, which may be due to a stronger influence of the interfaces on the overall nonradiative lifetime. The nonradiative lifetimes of all samples increase close to 1 μs and beyond for high injection, although the accuracy of the extracted lifetimes at higher injection levels (where the observed PDR-PL signal decreases) are not quantitatively accurate and therefore not included in Fig. 6. The drop in nonradiative lifetime beyond the radiative limit should not be interpreted quantitatively, since this is attributed to the Auger recombination (see Appendix A).

Overall, these results demonstrate the ability of the model to extract similar nonradiative lifetimes in the low injection regime for samples of various thicknesses using this measurement technique. The resulting nonradiative lifetime can also be used to separate the influences of interface and bulk recombination. This study is given in Appendix B. The assumption that the effective radiative efficiency reaches unity at high injection can be directly tested with this model. The relative effective radiative, SRH, and Auger recombination rates are compared as a function of carrier concentration, which shows the radiative rates approaching 99.5% (see

Appendix A). Thus, the assumption that the material reaches a purely radiative state under high injection has an uncertainty of 0.5%. The extracted SRH lifetimes of up to 1 μs at injection levels approaching this 99.5% purely radiative state can, therefore, be extracted with reasonable accuracy. Interestingly, the carrier concentration close to an injection of 4×10^{12} cm^{-3} (which is the injection level for GaAs solar cells at short-circuit current under standard testing conditions) falls in the regime where the nonradiative lifetime begins to increase. Therefore, as the applied bias is ramped from short circuit to open circuit conditions during a current–voltage measurement, the nonradiative lifetime will increase due to the injection of minority carriers. The observed increase in lifetime also supports the increased luminescence coupling observed in a tandem GaAs/GaAs laser power converter as a function of injection.[24]

V. CONCLUSIONS

The effective radiative efficiencies of four GaAs DHs of various thicknesses were measured for excitation intensities covering eight orders of magnitude using intensity-dependent photoluminescence. From these measurements, the nonradiative recombination lifetime was extracted as a function of excess carrier density using a steady-state carrier injection model. This model accounts for the effects of photon recycling through an effective radiative recombination coefficient which is found to depend on the optical properties including the thickness of the test structure. The model also assumes that the internal radiative efficiency approaches unity under the highest injection levels probed and amounts to an error of 0.5%. The GaAs DHs of different thicknesses and the same doping yield a constant nonradiative lifetime of 5.7 ± 0.5 ns for an excess carrier density below about 4×10^{12} cm^{-3}. In addition, it has been shown that the nonradiative lifetime increases for increasing injection level, which is believed to be due to trap saturation effects. This procedure can be applied, in principle, to any III-V semiconductor DHs with known absorption coefficients and can lead to a quantitative evaluation of sample material quality using simple measurements in parallel with some modeling efforts.

ACKNOWLEDGMENTS

APPENDIX A: RELATIVE RECOMBINATION RATES OVER INJECTION

The discussion regarding the observed drop in PDR-PL signal under the highest injection level merits further investigation. Considering the injected carrier concentration, one can analyze the distribution of carriers as a function of energy above the conduction band assuming Fermi-Dirac statistics and the effective density of states of both the Γ-band and the L-band of GaAs. This calculation is performed

in a similar manner to Ref. 28 using the density of states effective masses for bulk material.[14] One can thus directly gauge the carrier concentration with sufficient energy to fill the indirect L-band (which would experience a significantly lower radiative recombination probability). Together with the energy band diagram at the GaAs/AlGaAs interface, one can also gauge the concentration of carriers with energy sufficient to overcome the potential barrier of the DH. The indirect bandgap of $Al_{0.75}Ga_{0.25}As$ corresponds to the X-band, which has a 300 meV conduction band offset with respect to GaAs,[29] and increases to nearly 600 meV due to doping-induced band bending. In comparison, the indirect band of GaAs (L-band) is separated from the Γ-band by 285 meV.[14] Thus carriers are more likely to fill the indirect band of GaAs than escaping the DH by overcoming the AlGaAs potential barrier. Fig. 7(a) outlines the relative carrier concentration in the Γ- and L-bands (direct and indirect, respectively) as a function of laser intensity. One can observe that the band filling into the L-band is at most 0.15% at the highest injection levels probed. Fig. 7(b) reveals that the Auger recombination amounts to nearly 1.5% of the total recombination rates under the highest injection level probed (close to $10^{18} cm^{-3}$). Thus, the Auger recombination is mostly responsible for the observed drop of nearly 3% for the 1000 nm DH sample. Since the Auger recombination coefficients have
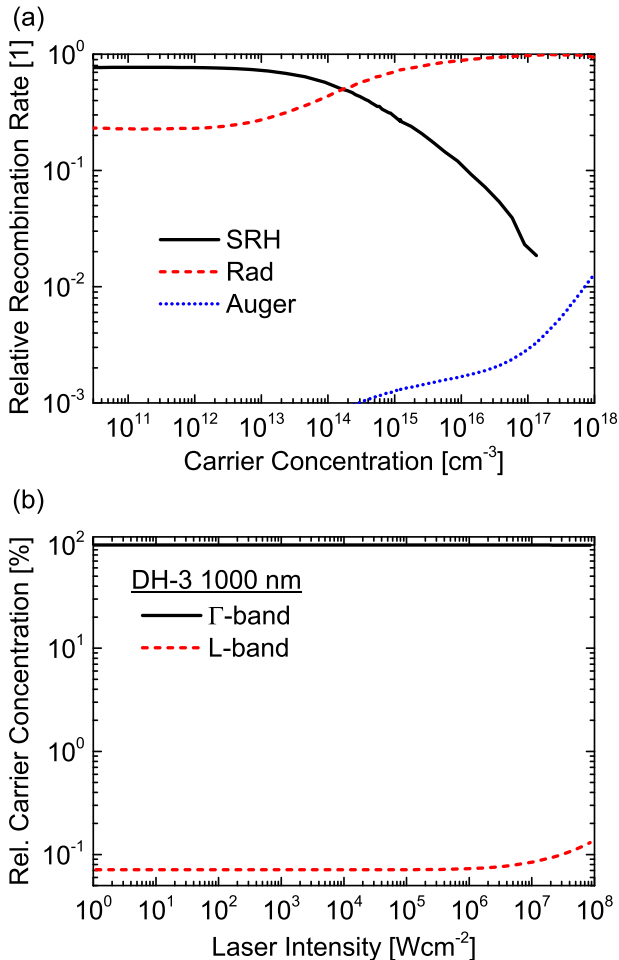
been reported to be between 10^{-30} cm^6 s^{-1} (Ref. 14) and $(7 \pm 4) \times 10^{-30}$ cm^6 s^{-1},[30] it is possible that the coefficients are slightly larger than those adopted in this study. The relative SRH recombination rate at high injection, where the system reaches close to 100% effective radiative efficiency, is not shown here. Furthermore, the highest relative effective radiative recombination rate achieved is 99.5%, which indicates a maximum uncertainty of 0.5% in the model's assumption of a 100% radiative state under high injection. Note that a 99.7% internal radiative efficiency for GaAs DHs has previously been reported.[17]

APPENDIX B: BULK AND INTERFACE RECOMBINATION

The surface recombination velocity can be extracted by performing a linear regression analysis on the inverse lifetime as a function of inverse thickness, or

$$\frac{1}{\tau} = \frac{1}{\tau_{rad}} + \frac{1}{\tau_{srh}} + \frac{2 \cdot srv}{d}, \qquad (B1)$$

where srv is the surface recombination velocity. The results are illustrated in Fig. 8(a) for an injected carrier concentration of $4 \times 10^{12} cm^{-3}$. The extracted surface

FIG. 7. (a) Modeled relative carrier distribution in the Γ- and L-bands in GaAs for increasing laser intensity. (b) Modeled relative radiative, SRH, and Auger recombination rates as a function of carrier concentration.
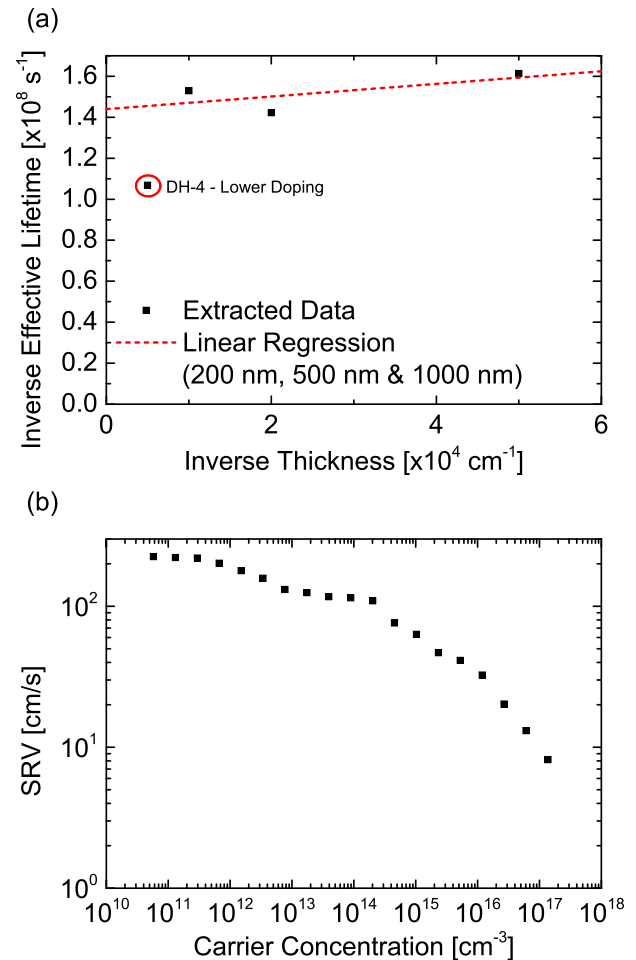

FIG. 8. (a) Inverse effective lifetime as a function of inverse thickness (Equation (B1)) for four GaAs DHs (200 nm, 500 nm, 1000 nm, and 2000 nm) at a carrier concentration of $4 \times 10^{12} cm^{-3}$ to extract the effective surface recombination velocity. (b) Extracted SRV as a function of injected carrier concentration.

recombination velocity, given by half of the slope, is 150 cm/s if one compares the thinnest samples which have a comparable doping concentration. Again, the lower doping of the 2000 nm sample (DH-4) implies that the surface recombination velocity and SRH lifetime will be different than in samples of higher doping and is therefore not used in the fit of Fig. 8(a). The extracted surface recombination is relatively low, which represents a high quality GaAs/AlGaAs interface. However, the uncertainty of this extracted value is relatively high, as can be seen by the fit to the inverse effective lifetime data. Several factors influence this accuracy, such as absorption data in the optical calculations, the doping concentration of the absorber layer, and the contribution of carriers generated in the barrier layers. The SRH bulk lifetime of the material at this particular injection of 4×10^{12} cm^{-3}, given by the intercept, is 6.9 ± 0.5 ns. This fitting procedure was also done as a function of injection level in order to extract the SRH lifetime and the surface recombination velocity as a function of injection, the latter of which is depicted in Fig. 8(b). The surface recombination velocity decreases as a function of increasing carrier concentration, which is an indication that traps are being saturated at the interfaces. When the system approaches an effective radiative efficiency of unity, however, the surface recombination velocity (similarly to the SRH lifetime) cannot be trusted quantitatively because the effective SRH recombination rate decreases to zero, which corresponds to zero surface recombination velocity (or infinite SRH lifetime). The shape of Fig. 8(b) may simply indicate different interface trap populations saturate at different injection levels. The uncertainty in the extracted surface recombination velocity is highest in the lowest injection regime and decreases as a function of carrier concentration.

[1]S. Chen, L. Zhu, M. Yoshita, T. Mochizuki, C. Kim, H. Akiyama, M. Imaizumi, and Y. Kanemitsu, Sci. Rep. **5**, 7836 (2015).

[2]J. F. Geisz, M. A. Steiner, I. Garcia, R. M. France, W. E. McMahon, C. R. Osterwald, and D. Friedman, IEEE J. Photovoltaics **5**, 1827 (2015).

[3]D. M. Tex, T. Ihara, H. Akiyama, M. Imaizumi, and Y. Kanemitsu, Appl. Phys. Lett. **106**, 013905 (2015).

[4]D. M. Tex, M. Imaizumi, and Y. Kanemitsu, Opt. Express **23**, A1687 (2015).

[5]O. D. Miller and E. Yablonovitch, "Photon extraction: the key physics for approaching solar cell efficiency limits," Proc. SPIE **8808**, 880807 (2013).

[6]O. D. Miller, E. Yablonovitch, and S. Kurtz, IEEE J. Photovoltaics **2**, 303 (2012).

[7]L. Zhu, C. Kim, M. Yoshita, S. Chen, S. Sato, T. Mochizuki, H. Akiyama, and Y. Kanemitsu, Appl. Phys. Lett. **104**, 031118 (2014).

[8]P. Asbeck, J. Appl. Phys. **48**, 820 (1977).

[9]M. A. Steiner, J. F. Geisz, I. Garcia, D. J. Friedman, A. Duda, W. J. Olavarria, M. Young, D. Kuciauskas, and S. R. Kurtz, IEEE J. Photovoltaics **3**, 1437 (2013).

[10]R. K. Ahrenkiel, B. M. Keyes, and D. J. Dunlavy, J. Appl. Phys. **70**, 225 (1991).

[11]E. Centurioni, Appl. Opt. **44**, 7532 (2005).

[12]W. Shockley and W. T. Read, Phys. Rev. **87**, 835 (1952).

[13]T. Tiedje, E. Yablonovitch, G. D. Cody, and B. G. Brooks, IEEE Trans. Electron Devices **ED-31**, 711 (1984).

[14]*Si, Ge, C (Diamond), GaAs, GaP, GaSb, InAs, InP, InSb*, edited by M. Levinshtein, S. Rumyantsev, and M. Shur (World Scientific Publishing, Singapore, 1996), Vol. 1.

[15]G. B. Lush, H. F. MacMillan, B. M. Keyes, D. H. Levi, M. R. Melloch, R. K. Ahrenkiel, and M. S. Lunstrom, J. Appl. Phys. **72**, 1436 (1992).

[16]T. Schmidt, A. Lischka, and W. Zulehner, Phys. Rev. B **45**, 8989 (1992).

[17]I. Schnitzer, E. Yablonovitch, C. Caneau, and T. Gmitter, Appl. Phys. Lett. **62**, 131 (1993).

[18]T. Kraus, O. Höhn, H. Hauser, and B. Bläsi, J. Appl. Phys. **115**, 053103 (2014).

[19]P. Würfel, *Physics of Solar Cells - From Principles to New Concepts* (Wiley-VCH, Weinheim, Germany, 2005).

[20]A. W. Walker, O. Höhn, D. N. Micha, F. Dimroth, B. Bläsi, and A. W. Bett, IEEE J. Photovoltaics **5**, 6802607 (2015).

[21]O. Höhn, T. Kraus, U. T. Schwarz, and B. Bläsi, "Photonics for solar energy systems V," Proc. SPIE **9140**, 91400B (2014).

[22]D. M. Whittaker and I. S. Culshaw, Phys. Rev. B **60**, 2610 (1999).

[23]L. Li, J. Opt. Soc. Am. **13**, 1024 (1996).

[24]A. W. Walker, O. Höhn, D. N. Micha, L. Wagner, H. Helmers, A. W. Bett, and F. Dimroth, J. Photonics Energy **5**, 053087 (2015).

[25]M. Wilkins, C. E. Valdivia, M. Gabriel, D. Masson, S. Fafard, and K. Hinzer, J. Appl. Phys. **118**, 143102 (2015).

[26]H. C. J. Casey and F. Stern, J. Appl. Phys. **47**, 631 (1976).

[27]M. P. Lumb, M. A. Steiner, J. F. Geisz, and R. J. Walters, J. Appl. Phys. **116**, 194504 (2014).

[28]R. Nagarajan, T. Kamiya, and A. Kurobe, IEEE J. Quantum Electron. **25**, 1161 (1989).

[29]*Ternary and Quaternary III-V Compounds*, edited by M. Levinshtein, S. Rumyantsev, and M. Shur (World Scientific Publishing, Singapore, 1999). Vol. 2.

[30]U. Strauss, W. W. Rühle, and K. Köhle, Appl. Phys. Lett. **62**, 55 (1993).